Impacts of interannual isoprene variations on methane lifetimes and trends

James Yoon

A thesis
submitted in partial fulfillment of the
requirements for the degree of

Master of Science

University of Washington

2025

Committee:
Alexander J. Turner
Joel A. Thornton
Abigail L. S. Swann

Program Authorized to Offer Degree:
Atmospheric and Climate Science

University of Washington

Abstract

Impacts of interannual isoprene variations on methane lifetimes and trends

James Yoon

Co-Chairs of the Supervisory Committee:
Alexander J. Turner
Atmospheric and Climate Science

Joel A. Thornton
Atmospheric and Climate Science

Methane is a potent greenhouse gas that has an atmospheric lifetime of 9-12 years due to its reaction with the hydroxyl radical (OH). Recent trends in methane indicate anomalously high methane growth in 2020, which has been attributed to a combination of increased wetland emissions and a decrease in OH from decreased anthropogenic nitrogen oxide (NO_x) emissions during the COVID-19 lockdowns. However, NO_x is not the only atmospheric species that affects global OH concentrations—isoprene, the most significant non-methane hydrocarbon by total emissions, is oxidized by OH, which can deplete OH during periods of high isoprene emissions. Using satellite isoprene retrievals from the Cross-track infrared sounder (CrIS) instrument, we find interannual variability in isoprene columns and anomalously high isoprene columns during 2020, coincident with anomalously high methane growth. Although isoprene is concentrated in source regions such as the Amazon, its atmospheric oxidation produces carbon monoxide, which can be transported over longer distances and thus impact the global atmospheric oxidative capacity. Elevated isoprene concentrations may have contributed 13% (bounds: 10% - 28%) of the total methane growth in 2020 if we assume no change in NO_x emissions between 2019 and 2020. Given that COVID-19 lockdowns also decreased anthropogenic NO_x emissions during this same period, this estimate of isoprene

emissions on the methane lifetime during 2020 is an upper-limit, and the resulting change in the oxidative capacity may be sensitive to whether isoprene emissions or NO emissions drove this isoprene anomaly. This study illustrates how the biosphere may impact the atmospheric oxidative capacity and, in turn, the methane lifetime through interannual changes in biogenic emissions that are forced by meteorological and climate variability.

TABLE OF CONTENTS

LIST OF FIGURES

LIST OF TABLES

DEDICATION

For my 할머니, 이옥란.

Chapter 1

INTRODUCTION

Methane (CH_4) is the second most important greenhouse gas behind carbon dioxide and is 84 times more potent than carbon dioxide over a 20-year time horizon [24]. It is emitted from both natural and anthropogenic sources, including oil & gas infrastructure, landfills, feedlots, and wetlands, while its dominant sink is oxidation initiated by the hydroxyl (OH) radical with an atmospheric lifetime of 9–12 years [22]. Therefore, variations in both methane emissions and OH concentrations, [OH], can impact observed methane mixing ratios. The latter may have been important for the rising methane mixing ratios observed after 2007, which previous work has attributed to decreased [OH] and an increase in the methane lifetime, among other hypotheses (e.g., [26, 21]).

In 2020 and 2021, global methane mixing ratios grew at unprecedented rates (hereby referred to as "methane acceleration"). Previous studies have attributed this trend to increased emissions or decreased [OH] from lower nitrogen oxide (NO_x) emissions during the COVID-19 lockdowns [11]. Peng et al. (2022) attributed the methane acceleration to both increased wetland emissions and decreased OH concentrations due to NO_x changes during the COVID-19 pandemic, with a [OH] decrease of $1.6 \pm 0.2\%$ contributing $53 \pm 10\%$ of the observed methane trend [20]. Other studies argue that the methane acceleration was largely due to wetland emissions with little impact from OH changes: for example, Feng et al. (2022) attributed just 16% of the acceleration to OH [5].

NO_x emissions are not the only factor determining tropospheric [OH] and the global methane sink: global [OH] also generally increases with actinic flux, ozone, and atmospheric water vapor, and decreases with volatile organic compound (VOC) emissions. Isoprene is a biogenic VOC (BVOC) released largely from broadleaf deciduous trees in response to high

light and high temperature conditions [28, 1, 33] in large enough quantities to potentially affect global [OH]. By total emission flux, isoprene is the most significant non-methane VOC, with estimates of 440-660 Tg C yr^{-1} emitted into the atmosphere as isoprene [7]. Once in the atmosphere, isoprene is predominantly oxidized by OH, with typical lifetimes on the order of 1 hour, creating organic products like isoprene epoxydiols that are involved in photochemical smog formation and secondary organic aerosol formation [2, 9]. Due to its large reaction rate constant towards OH, high isoprene emissions can deplete local [OH], which in turn can extend isoprene's own lifetime. Bates & Jacob (2019) found that implementing isoprene chemistry via the reduced Caltech isoprene mechanism into the chemical transport model GEOS-Chem resulted in 70% reductions to local [OH] in the Amazon and equatorial Africa, as well as a 12% increase in the tropospheric methane lifetime [2]. Isoprene impacts are therefore not restricted to its source regions but can impact global [OH]. As isoprene emissions are driven by ecosystem characteristics, regional climate, and weather, global [OH] variability can therefore be due in part to processes or conditions that alter isoprene emissions.

Isoprene emissions in chemical transport (e.g. GEOS-Chem) or chemistry-enabled climate models (e.g. CAM6-Chem) are often parameterized through MEGAN (Model of Emissions of Gases and Aerosols from Nature) v2.1, which calculates isoprene emissions as the product of a vegetation-specific emission factor; the fractional area covered by that vegetation type; and an activity factor that depends on isoprene's dependence on light, temperature, soil moisture, CO_2, leaf age, and leaf area index [7, 8, 4]. To provide top-down space-based constraints on isoprene emissions, previous studies have traditionally used formaldehyde in isoprene source regions as an isoprene proxy, since formaldehyde is a product of isoprene oxidation with a globally-averaged yield of 22% per carbon [2, 13, 12, 19, 18]. However, using formaldehyde as a proxy in low [OH] regions could result in smoothing caused by advection [25]. In addition to smoothing errors, the formaldehyde yield from isoprene oxidation increases with local NO_x concentrations, and fires or VOCs like methanol are other sources of formaldehyde independent of isoprene [32]. In 2020, Wells et al. developed novel isoprene satellite measurements from the Cross-track infrared sounder (CrIS) instrument using a brightness

temperature difference and an artificial neural network; in 2022, this algorithm was revised to use a hyperspectral index [31, 30, 23]. Recently, these retrievals have been used to investigate multiyear trends in the atmospheric oxidative capacity over the Southeastern United States and ENSO-driven OH variability in Papua New Guinea [23].

The largest isoprene anomalies in the 9-year CrIS record occur in late-2019 and continue through 2020 (Fig. 3.1a). This anomaly is not well-represented in GEOS-Chem with MEGAN-generated BVOC emissions (Fig. 3.1a), and these isoprene column anomalies roughly coincide with the methane acceleration. Here we investigate whether elevated isoprene levels driven by higher isoprene emissions could indirectly contribute to the observed methane acceleration by modulating [OH].

Chapter 2

METHODS

2.1 Model runs

All model runs were conducted using GEOS-Chem v14.1.1 with offline BVOC emissions on a 4° latitude by 5° longitude grid, spanning an eight year period from 2012–2020 to temporally coincide with the CrIS dataset. The first five months (February–June 2012) were considered spin-up and were thus removed from the analysis. In total, three model simulations were conducted: 1) a baseline simulation with offline MEGAN emissions, 2) an isoprene climatology simulation that removed interannual variations in isoprene emissions by replacing the MEGAN emissions at each latitude–longitude box with its monthly 2012–2020 climatology, and 3) a simulation where isoprene emissions were scaled to better match the CrIS retrievals. Anthropogenic NO emissions were taken from the CEDSv2 inventory, with 2020 anthropogenic NO emissions set at 2019 emissions as 2020 data was not available at the time of the runs. Isoprene chemistry in GEOS-Chem 14.1.1 was parameterized by the Bates & Jacob (2019) mechanism [2].

For simulation 3, we iteratively scaled the isoprene emissions to better match the CrIS retrievals. The iteration was necessary to account for the non-linear relationship between isoprene emissions and the simulated concentrations due to its feedback on [OH]. Preliminary

Table 2.1: Summary of GEOS-Chem simulations

Simulation	**Isoprene Emissions**
1	Offline MEGAN emissions ("`baseline`")
2	Offline MEGAN emissions but set at monthly climatology (2012-2020) at each latitude-longitude ("`isoprene_climatology`")
3	Iteratively scaled MEGAN emissions to better match CrIS isoprene retrievals (`scaled_isoprene`)

scalings indicated that a doubling of isoprene emissions over the Amazon and equatorial Africa resulted in a three-fold increase in modeled isoprene columns, which was due to isoprene's feedback with local [OH]. As isoprene emissions increase, isoprene can deplete local [OH], which increases its own lifetime. To account for this feedback, our first iteration (run 3a) scaled MEGAN isoprene emissions at each latitude-longitude box for every month using Eqn. 2.1.

$$\eta_1 = 1 + \frac{1}{2}\left(\frac{\mathrm{CrIS}_{\mathrm{isoprene}}}{\mathrm{GC}_{\mathrm{base,isoprene}}} - 1\right) \tag{2.1}$$

In Eqn. 2.1, η_1 is the scaling factor for the offline MEGAN emissions at each latitude-longitude, $\mathrm{CrIS}_{\mathrm{isoprene}}$ is the CrIS satellite isoprene column retrieval (in molecules cm^{-2}), and $\mathrm{GC}_{\mathrm{base,isoprene}}$ is the isoprene column simulated by the baseline GEOS-Chem run. This ensured emissions were only changed in regions with GEOS-Chem isoprene columns that deviate from CrIS observations. The $\frac{1}{2}$ can be thought of as a "feedback" factor, originating due to the empirical 3:2 relationship between isoprene columns and emissions. Scaling factors were first calculated on GEOS-Chem's 4° x 5° grid and then linearly interpolated to match GEOS-Chem's 0.5° x 0.625° offline BVOC emissions. This first iteration generally overestimated isoprene, particularly in the Northern mid-latitudes.

The second iteration improved on the first iteration by then considering regional changes in [OH]. For each region delineated in Figure 2.1, the change in isoprene emissions (η_1 in Eqn. 2.1) was compared to the corresponding change in modeled isoprene columns between the first iteration and the baseline simulation:

$$\eta_2 = \frac{\mathrm{CrIS}_{\mathrm{isoprene}}}{\mathrm{GC}_{\mathrm{base,isoprene}}} \times \frac{E_1/E_{\mathrm{base}}}{C_1/C_{\mathrm{base}}} \tag{2.2}$$

In Eqn. 2, E_1 and E_{base} represent the isoprene emissions in the first iteration and in the baseline simulation, and C_1 and C_{base} represent the modeled isoprene columns (in molecules cm^{-2}) from those same runs. The ratio ($\frac{E_1/E_{\mathrm{base}}}{C_1/C_{\mathrm{base}}}$), which is equivalent to $\frac{\eta_1}{C_1/C_{\mathrm{base}}}$, was computed for every year and represents the increase in isoprene solely due to isoprene-OH feed-

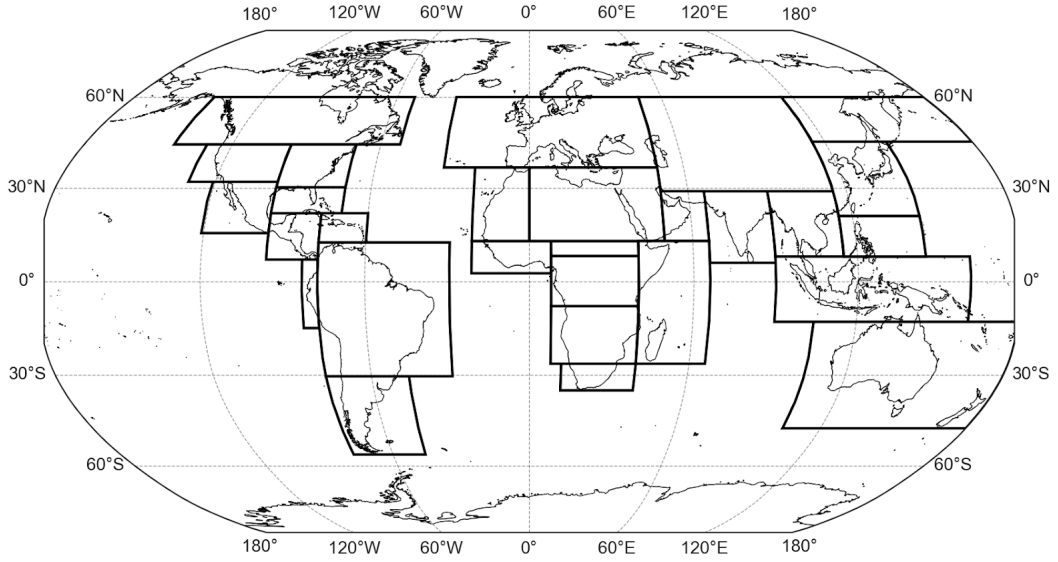

Figure 2.1: Geographic regions used in the second scaling to compute regional scaling factors. Areas above 60° were not present in the CrIS observations and were set to default offline MEGAN isoprene emissions.

back (i.e. regional feedback factors).

To estimate uncertainty in the 2020 methane lifetime impact, we note that the uncertainty in simulation 3 largely originates from the regional feedback factors used in the second iteration, i.e. the $(\frac{E_1/E_{\text{base}}}{C_1/C_{\text{base}}})$ ratio in Eqn. 2.2. This regional ratio serves a similar purpose to the global $\frac{1}{2}$ factor present in Eqn. 2.1, as they both modulate the isoprene based on the OH feedback. We thus set the upper and lower bounds of isoprene's impact by scaling isoprene emissions again using Eqn. 2.1, but replacing the $\frac{1}{2}$ global feedback factor with the 16th and 84th percentiles of the $(\frac{E_1/E_{\text{base}}}{C_1/C_{\text{base}}})$ ratios used in the second iteration. These corresponded to $\frac{1}{6}$ and $\frac{1}{2}$, respectively (Fig. 2.2), and thus the first iteration (run 3a) served as the upper bound on isoprene emissions. Percentiles were calculated by compiling all feedback factors at every gridpoint between 2012–2020.

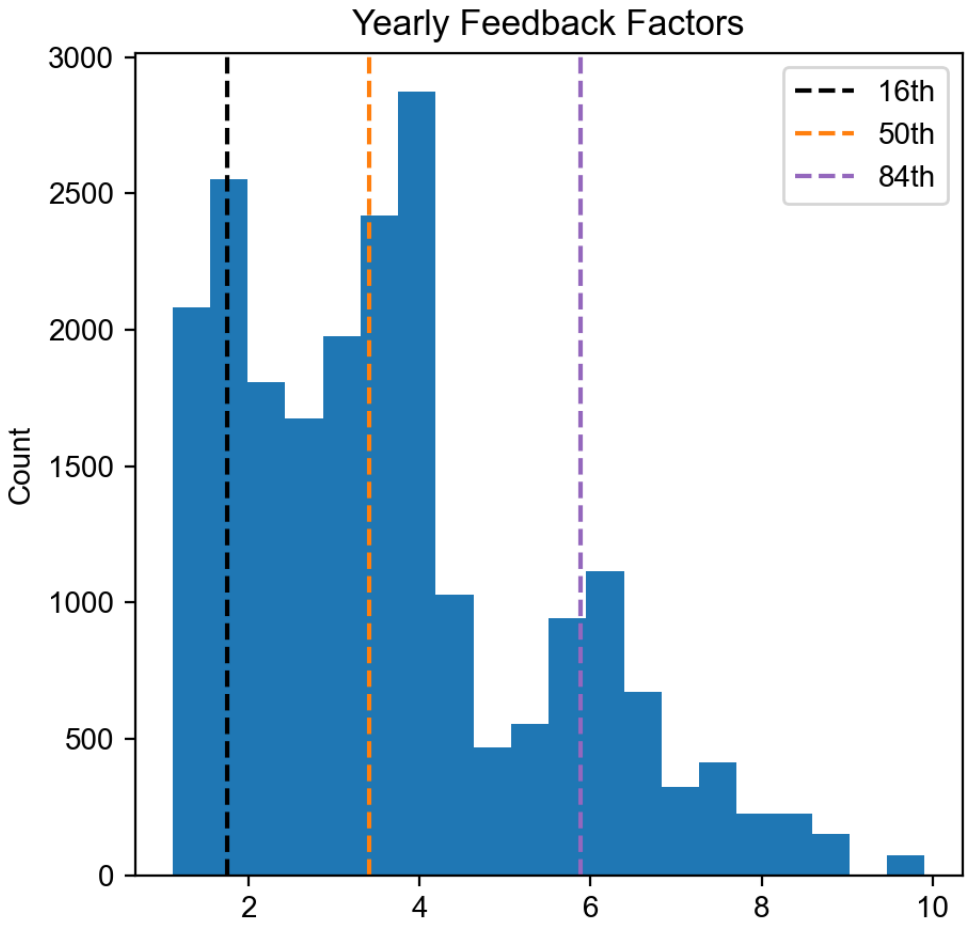

Figure 2.2: Histogram of 2012–2020 feedback factors used in the second scaling. The x-axis represents the denominator of the feedback factor (e.g. the $\frac{1}{2}$ in Eqn. 2.1 would translate to 2 in this figure). Using these reciprocals, the 16th percentile was 1.75 and the 84th percentile was 5.89. The final global feedback factors used for uncertainty analysis were $\frac{1}{2}$ and $\frac{1}{6}$ (denominators rounded to the higher integer), as this ensured a more conservative scaling. Higher feedback factors mute the scaling factor, resulting in a smaller change in isoprene columns.

2.2 Satellite comparisons

Globally-averaged modeled isoprene columns from GEOS-Chem were land-masked before comparing with 4° x 5° bilinearly-regridded CrIS observations. Further information on the CrIS isoprene retrievals are described in Fu et al. (2019) and Wells et al. (2020, 2022) [6, 31, 30].

Carbon monoxide (CO) satellite columns were taken from L3 near and thermal infrared radiances from MOPITT (MOP03JM v.9), which was processed onto a 1° x 1° grid [15]. NO_2 retrievals were taken from the L3 OMNO2d product, which contained cloud-screened total and tropospheric NO_2 columns on a 0.25° x 0.25° grid [17]. Monthly satellite columns (taken between 12:00 and 15:00 LT) from the SatDiagn output were used when comparing satellite retrievals with model output.

To account for MOPITT's averaging kernel, which is most sensitive in the mid-troposphere, GEOS-Chem CO columns were transformed into values analogous to MOPITT's columns (C_{comp}) using the a priori CO columns and the provided averaging kernel as:

$$C_{comp} = C_a + A(x_{\text{modeled}} - x_a) \tag{2.3}$$

In Eqn. 2.3, x_{modeled} is the modeled vertical profile interpolated to MOPITT's pressure levels; x_a and C_a are the a priori profile and columns, respectively; and A is the averaging kernel.

2.3 Modeling the impact on atmospheric methane

To estimate isoprene's global impact on the 2020 methane acceleration, we used a two-box CH_4-OH model to calculate Northern and Southern hemisphere methane concentrations at various OH concentrations with interactive OH [26, 16]. Further information about the model and its datasets can be found in Turner et al. (2017) and Nguyen et al. (2020).

We parameterized methane emissions to be constant prior to 2007 followed by a linear increase between 2007 and 2019, and then constant in 2020. While keeping methane emissions

at 2019 levels in 2020, we implemented a stepwise decrease in the OH source. The OH source in the two-box model was reduced by the same percent decrease in tropospheric [OH] between 2020 and 2019, as calculated in GEOS-Chem, for simulation 3 relative to simulation 2. By taking the difference between simulations 3 and 2, we isolate the impact of isoprene emissions alone on the oxidative capacity. This output was compared to the simulated methane concentrations using Peng et al. (2022)'s 1.6% decrease in OH, which was responsible for approximately half of the methane growth; a 3% decrease in OH, which should correspond to a scenario where all of the methane growth was caused by OH changes; and NOAA methane observations [10].

Chapter 3

RESULTS

CrIS measurements indicate a period of anomalously high isoprene in 2020, with anomalies calculated using the 2012-2020 monthly mean at each CrIS grid point as the climatology. Fig. 3.1a is a Hovmoller diagram that shows that much of this isoprene increase was located in the tropics (-20 to 20° latitude). Here, we investigate the impact this anomaly has on the oxidative capacity under the potential hypothesis that the CrIS isoprene column anomaly was driven by isoprene emissions. The potential impacts of NO_x emissions and isoprene-NO_x interactions are discussed later.

Baseline model simulations (baseline run with offline MEGAN emissions) underpredicted global averaged isoprene observed from CrIS by 50%. Our scaling (see Methods) of modeled isoprene emissions (`scaled_isoprene`) improved modeled global land isoprene columns to better match CrIS satellite observations, as shown in Figure 3.1b. The scaled isoprene rarely exceeded observed CrIS isoprene except in late 2016 and late 2020, and generally underestimated the early isoprene seasonal peak, which may be due to the isoprene-[OH] feedback ratio in the scaling being computed on yearly timescales. The discrepancy in modeled-observed isoprene was highest in 2015 and 2019. Nevertheless, the `scaled_isoprene` run was generally able to reproduce the satellite isoprene record from CrIS.

Additionally, scaling isoprene (`scaled_isoprene`) also altered the modeled seasonal cycle to better match CrIS's seasonal cycle due to increased isoprene emissions from areas such as equatorial Africa and the Maritime Continent. It also decreased the impact of a simulated isoprene hotspot in the southwestern Amazon while increasing the influence of other regions in the Amazon basin, namely the northern Amazon. These spatial trends are consistent with results from Wells et al. [31].

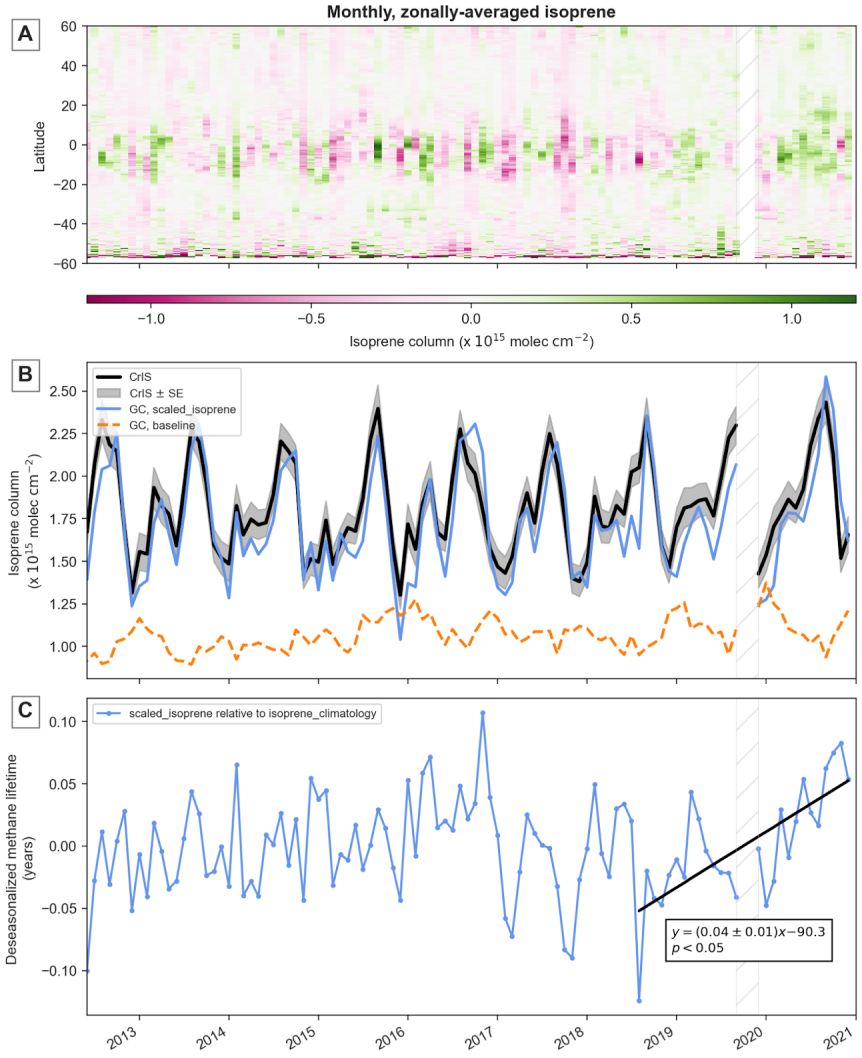

Figure 3.1: Time series analysis of isoprene and the methane lifetime. Hatched lines cover October–November 2019, which is due to anomalously high isoprene across all latitudes that may be an artifact of the background calculation. (a) Hovmoller diagram with CrIS isoprene anomalies at each latitude between July 2012 and December 2020. Each latitude gridbox spans 0.5 degrees, and anomalies were calculated relative to a monthly climatology at each gridbox. (b) Time-series of globally-averaged isoprene columns from the `baseline` GEOS-Chem run (dashed orange), `scaled_isoprene` GEOS-Chem run (solid light blue), and the CrIS instrument (solid black). The base run underpredicted CrIS columns, while the scaled run brings GEOS-Chem more in alignment with satellite observations. Furthermore, the `scaled_isoprene` run has a different seasonal cycle than the baseline run, with the former peaking in mid-year and the latter peaking in January. This new seasonal cycle in the `scaled_isoprene` simulation better matches the CrIS measurements. (c) Methane lifetimes for the `scaled_isoprene` (light blue) simulation relative to `isoprene_climatology`, which had no interannual variations in isoprene emissions. The scaled run showed an increase in methane lifetimes in 2019 and 2020 that is coincident with the 2020 methane acceleration.

Methane lifetimes increased by up to 0.8 years between the isoprene climatology and the scaled GEOS-Chem run. Due to isoprene's new seasonal cycle when emissions are scaled to match CrIS retrievals, the change in methane lifetimes also had an annual cycle which spiked in September and October. We also find interannual variation in methane lifetime (Figure 3.1c). In 2019 and 2020, higher methane lifetimes of up to an additional 0.1 years occurred in the `scaled_isoprene` run that did not appear in the base run. Although this isoprene-driven change in methane lifetimes is comparable in magnitude to other time periods (e.g. 2016), this 2019–2020 change represents a coherent, linear trend that is coincident with 2020's anomalously high methane growth.

3.1 Role of carbon monoxide

The oxidation of isoprene produces a range of oxygenated organic carbon products, e.g., formaldehyde, which in turn can be oxidized to form carbon monoxide (CO) and eventually CO_2. Here, we find that less than half of the global [OH] decrease is due to the direct oxidation of isoprene, but instead rather due to its subsequent oxidation products which are themselves removed by OH. Figure 3.2 shows the contribution of each species in the isoprene oxidation cascade to global OH depletion, with all column reaction rates reported as the difference between the `scaled_isoprene` and `baseline` runs. We observe that 30-70% of the increased oxidation is due to the CO + OH reaction, with its maximum fractional impact occurring during winter in the Northern hemisphere. Outside of isoprene and CO, other VOCs produced downstream of isoprene oxidation, such as methyl vinyl ketone (MVK) and methacrolein (MACR), also significantly impact the net OH loss, with these additional oxidation products accounting for up to 30% of the OH loss during boreal summer.

Interestingly, CO's contribution to the global OH decrease exceeds that of isoprene itself, and the timing lags the isoprene + OH reaction, as CO is produced downstream and has a lifetime of 1 month. This increased CO can be transported over longer distances than isoprene, which allows isoprene to have an impact on the global atmospheric oxidative capacity—beyond only affecting OH locally over isoprene source regions. Since much of inter-

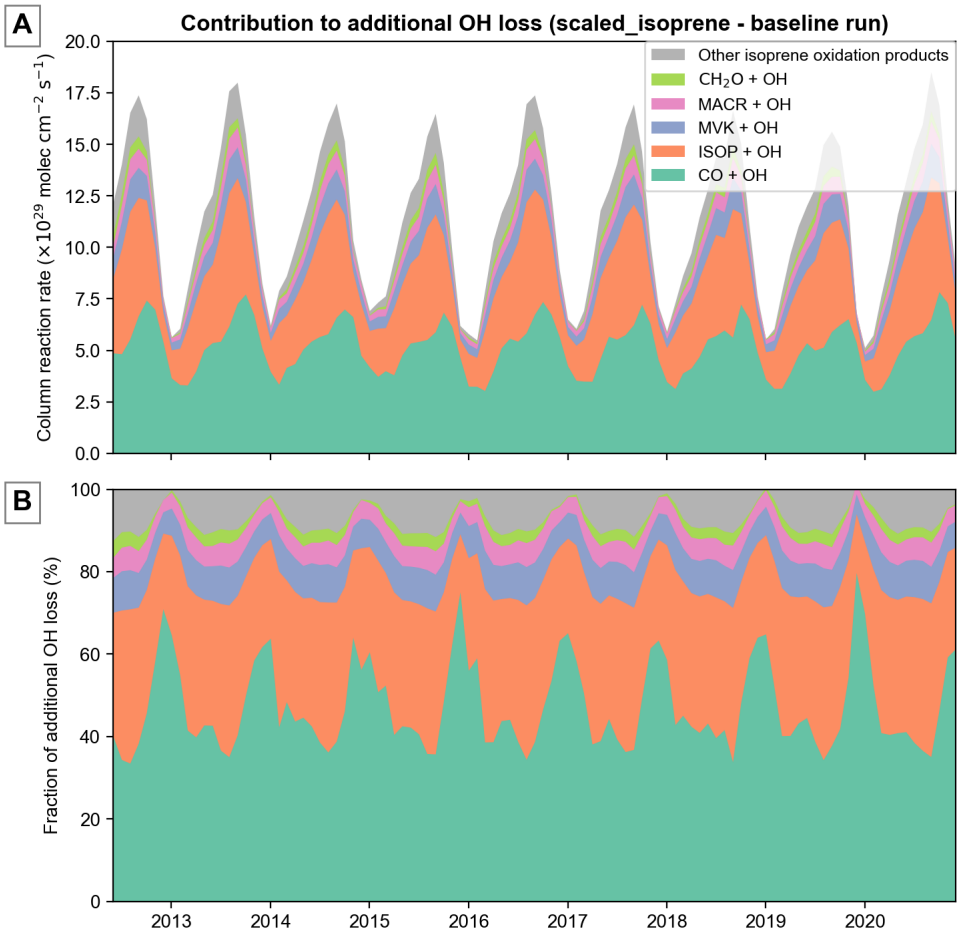

Figure 3.2: The contribution of various species to the global OH decrease observed between the `scaled_isoprene` and `baseline` runs via faster VOC + OH reactions. (a) Shows the change in column-integrated reaction rates. (b) Fractional contribution of each species + OH reaction to the additional OH loss. CO + OH is as significant as isoprene + OH on a global scale, and its delayed peak relative to isoprene + OH's peak is due to the chemical processing required to convert isoprene to CO via oxidation.

model variability in [OH] predictions is caused by variability in the oxidation efficiency—the fraction of a VOC (e.g. isoprene) oxidized to CO—OH loss from isoprene emissions is likely sensitive to a model's isoprene and VOC oxidation mechanism [14].

Increased isoprene oxidation increases the abundance of CO in the model, raising the question: "do independent observations of CO support this increased burden?" To assess this question, we compared the model simulations to MOPITT satellite observations of CO. Figure 3 shows the globally-averaged CO concentrations from MOPITT, the `baseline` simulation, and the `scaled_isoprene` simulation. As with isoprene, the `baseline` simulation underpredicts the satellite observations of CO from MOPITT. The `scaled_isoprene` run shows better agreement with MOPITT retrievals. The mean CO in the scaled run generally agrees with the observations from MOPITT, although there are temporal variations in the MOPITT observations that are not captured by the model. Nevertheless, the improved agreement between carbon monoxide from MOPITT and GEOS-Chem solely by changing isoprene emissions supports our isoprene scaling. Although the discrepancies in the seasonal cycle indicate some error in the isoprene scaling, the increase in CO is plausible given independent satellite measurements.

3.2 Impact on methane growth

As mentioned above, 2020 exhibited the largest methane growth rates ever observed in the in-situ record going back to 1983. As such, there has been much speculation about the cause of this methane acceleration. For 2020, the MEGAN model predicted a decrease in isoprene emissions, while CrIS satellite data show an increase in isoprene columns relative to previous years in the Amazon and Maritime Continent. We find a 0.4% decrease in global tropospheric [OH] from 2019-2020 in `scaled_isoprene` compared to the `isoprene_climatology` simulation. On the other hand, our baseline simulation shows a 0.1% increase in [OH] when compared to `isoprene_climatology`. Given that methane lifetime increased and that [OH] decreased, we attribute these modeled [OH] changes to interannual isoprene variations and the subsequent oxidation cascade.

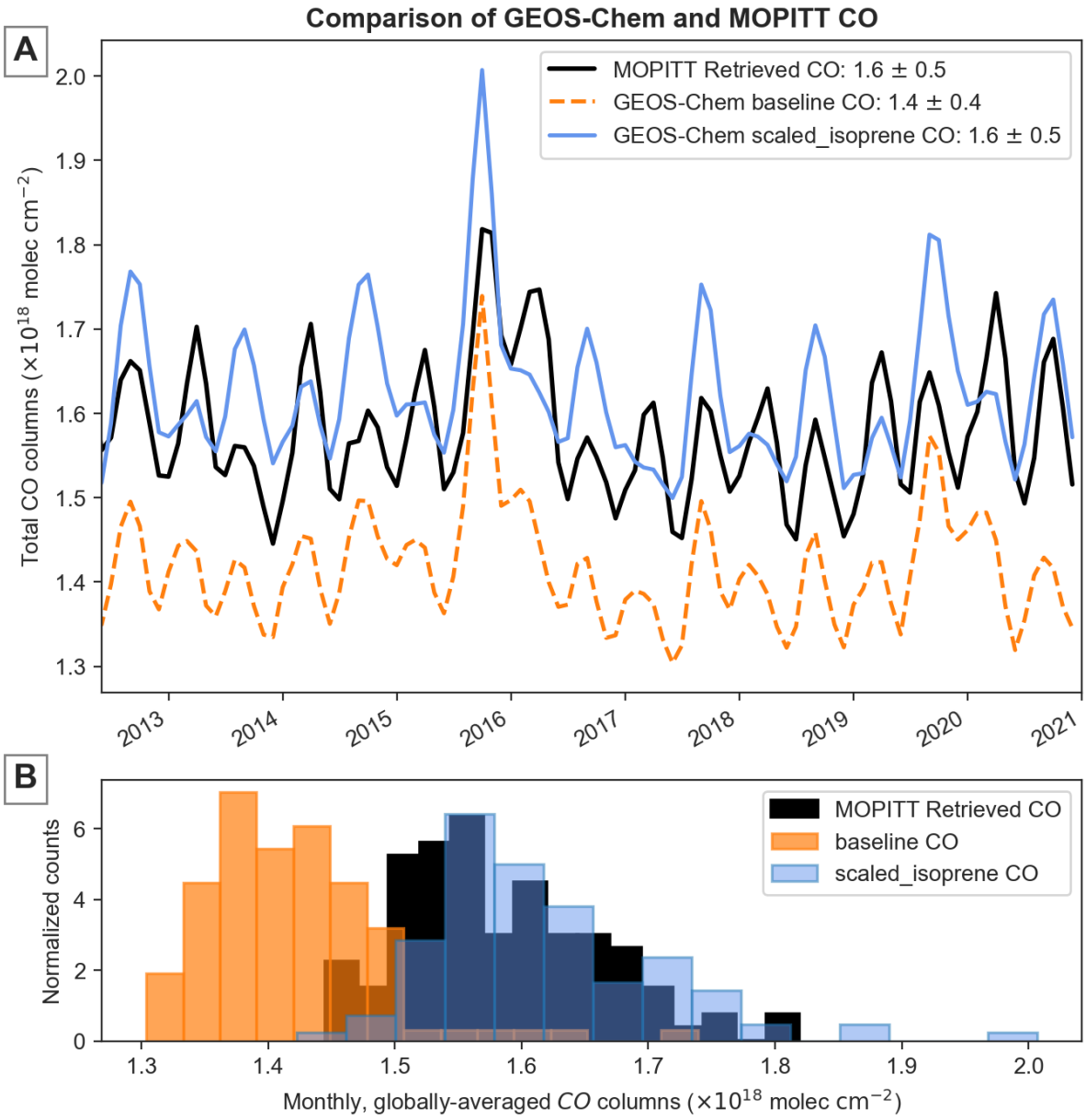

Figure 3.3: Comparison of carbon monoxide from GEOS-Chem and MOPITT. (a) Time-series of globally-averaged CO columns processed through the MOPITT averaging kernel from the baseline and `scaled_isoprene` GEOS-Chem runs, compared to the MOPITT total daytime CO columns. The enhanced isoprene from the scaled run translated to a baseline CO mean that was more in alignment with MOPITT than the base run. Uncertainties are reported as 1 standard deviation. (b) Histogram of monthly, globally-averaged CO columns. The difference in CO columns between both GEOS-Chem runs and the MOPITT CO retrievals was statistically significant ($p < 0.05$), but the mean CO is closer in agreement with MOPITT retrievals in the `scaled_isoprene` simulation than the `baseline` simulation.

To quantify how this change in tropospheric [OH] impacts atmospheric methane concentrations, we implemented a stepwise [OH] change into the two-box CH_4-OH model originally developed by Turner et al. [26]. This stepwise change in the box model was set as the 2020-2019 percent change in hemispheric tropospheric [OH] in the `scaled_isoprene` GEOS-Chem simulation. We then compared the change in methane diagnosed from the two-box model to that caused by the 1.6% decrease in tropospheric OH from Peng et al., and found that a theoretical 3% decrease in OH would explain all of 2020's methane growth (Fig. 3.4). This result agreed well with Peng et al. 's estimates, with a 1.6% decrease in OH also explaining approximately half of the methane growth in our two-box model. We note the hemispheric difference in the *in-situ* methane observations: both hemispheres experienced similar methane growth rates in magnitude, but observations indicate that the Southern hemisphere's methane growth reached a peak in early 2021, versus the Northern hemisphere's consistently elevated methane growth throughout 2020. Nevertheless, a 3% decrease in OH corresponded to the maximum magnitude of methane growth during the 2020-2021 period. Relative to the 3% [OH] decrease, we find that isoprene alone could account for 13% of the methane growth (bounds: 10% - 28%) if the anomalously high isoprene columns observed in 2020 were solely driven by isoprene emissions (Fig. 3.5).

Our results assume that 2020's isoprene anomalies were driven by isoprene emissions rather than changes in [OH] from NO_x, which would affect isoprene's lifetime. This assumption arises because our simulations do not consider changes in anthropogenic NO_x; modeled 2020 anthropogenic NO_x emissions were set to the 2019 values. In 2020, COVID-19 lockdowns decreased tropospheric NO_x columns through lower anthropogenic emissions [3, 29], and thus some of these isoprene and OH anomalies may be due to decreasing NO_x during this period. OMI NO_2 columns show that anthropogenic NO_x largely decreased in the Northern Hemisphere mid-latitudes, which is not spatially co-located with the large tropical isoprene sources found in this study [17]. Although changes in NO_x may propagate over long distances through changes in longer-lived species or peroxyacetyl nitrates (PANs), our sensitivity studies that decreased anthropogenic NO emissions by the observed change in OMI NO_2 columns

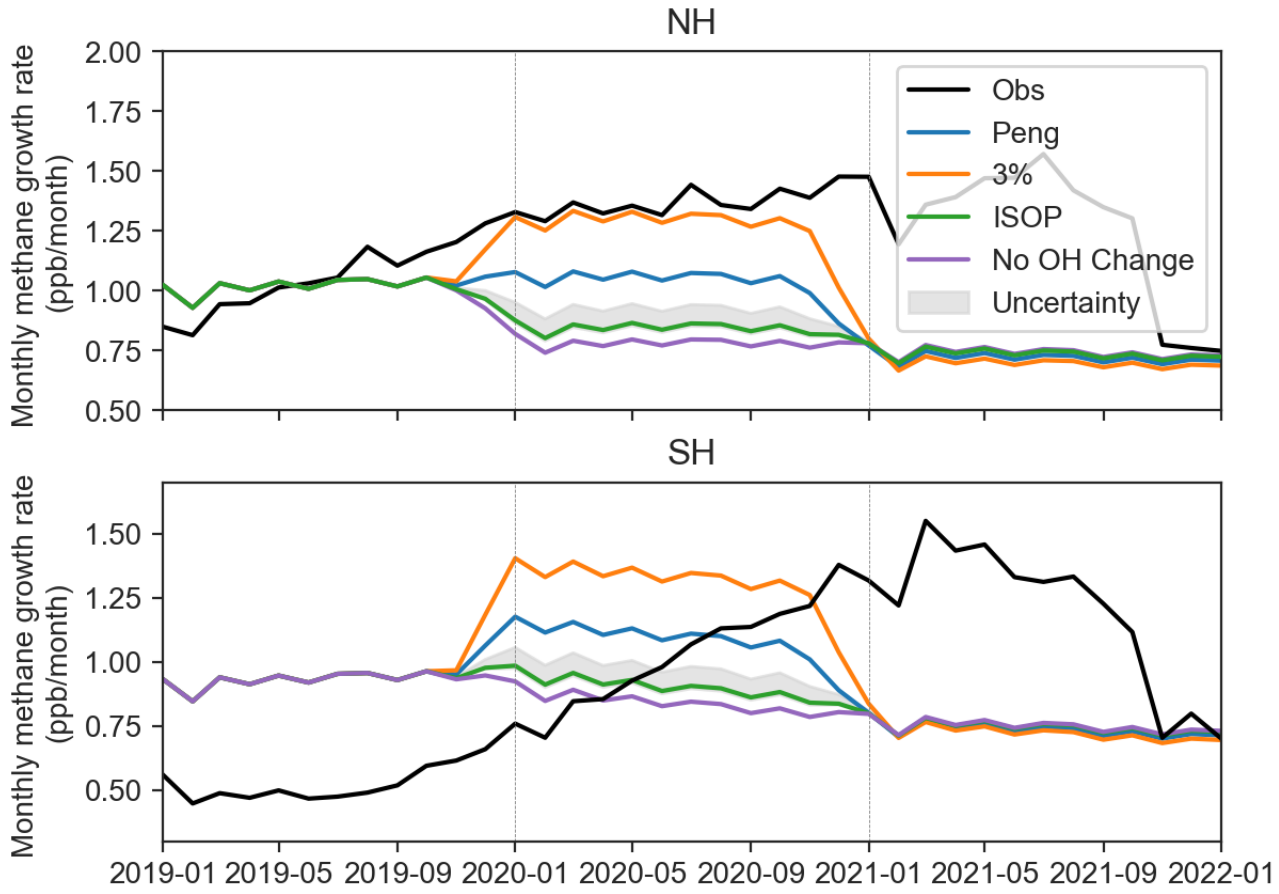

Figure 3.4: Time series of methane growth rates obtained from NOAA global observations (black) [10] and the Turner et al. two-box model [26]. The purple line represents the methane if there were no stepwise decrease in OH during 2020, while the Peng (blue) and 3% (orange) line represent the methane resulting from a 1.6% and 3% OH decrease in both hemispheres. The green line (ISOP) represents the methane if it experienced the same OH decrease between 2020 and 2019 as it did in simulation 3, and the uncertainty bounds are quantified using the OH differences in the GEOS-Chem uncertainty runs.

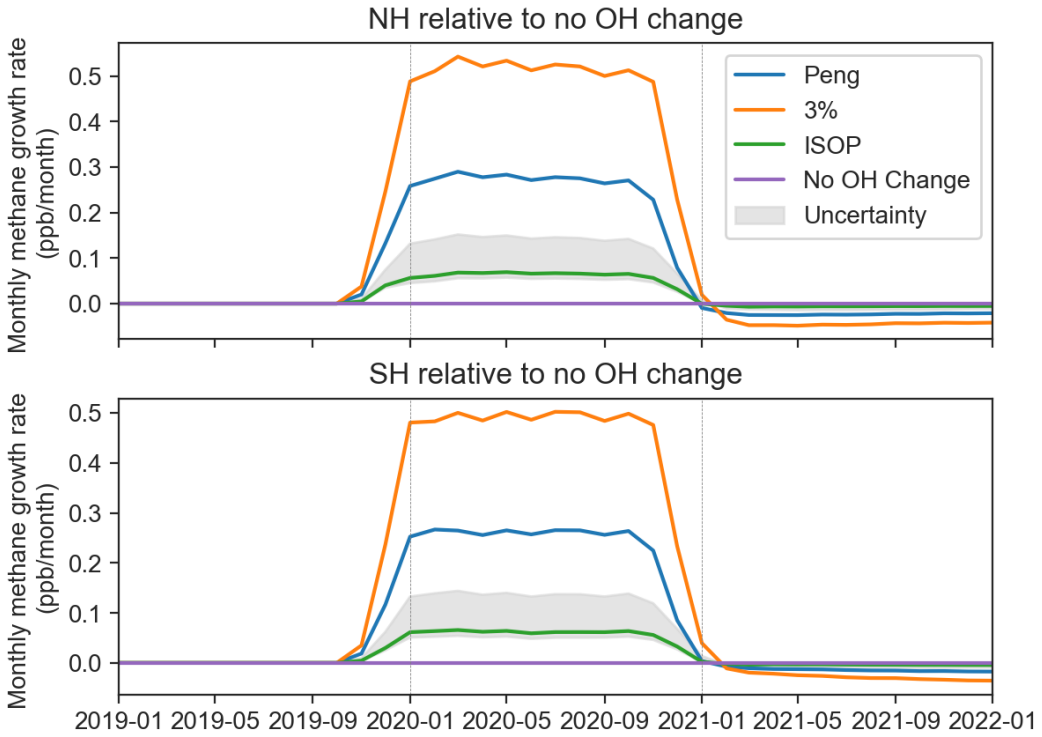

Figure 3.5: Same as Figure 3.4, but with all runs being shown relative to the no OH change run (purple).

between 2019 and 2020 suggest that the impact of these NO changes is mostly restricted to areas near large cities in the tropics, such as Bogotá, Singapore, and Jakarta. Furthermore, the isoprene anomaly lasts until the end of the year, while the COVID-19 NO_x decreases were largely during the first half of the year [11]. Nevertheless, identifying the cause of this 2020 isoprene anomaly is crucial, as it determines the mechanism through which [OH] impacts methane lifetimes.

Alternatively, changes in natural NO_x sources not directly related to the COVID-19 lockdowns, like soil or lightning NO_x, can impact isoprene columns in areas like the Maritime Continent, but more work needs to be done to determine the sensitivity of isoprene columns to each NO_x source. Nevertheless, even if NO_x drove much of these 2020 isoprene column anomalies, the magnitude of the OH perturbation is still sensitive to isoprene concentrations due to changes in chemistry [32]. For instance, the 2019-2020 increase in methane lifetime with the same COVID-19 NO_x sensitivity perturbation was higher by 1.2x in the `scaled_isoprene` run than the baseline run, indicating that higher mean global isoprene emissions may amplify NO_x's impact on [OH] (Fig. 3.6). It is important to note that the influence of NO_x on isoprene is highly dependent on the identity of the oxidation products and thus the model's chemical mechanism. The formation of certain isoprene hydroxynitrates and their rapid hydrolysis into HNO_3 may cause permanent NO_x loss in regions with changing NO emissions even with constant isoprene emissions, thus impacting how the isoprene-NO_x relationship influences OH and the oxidative capacity [27].

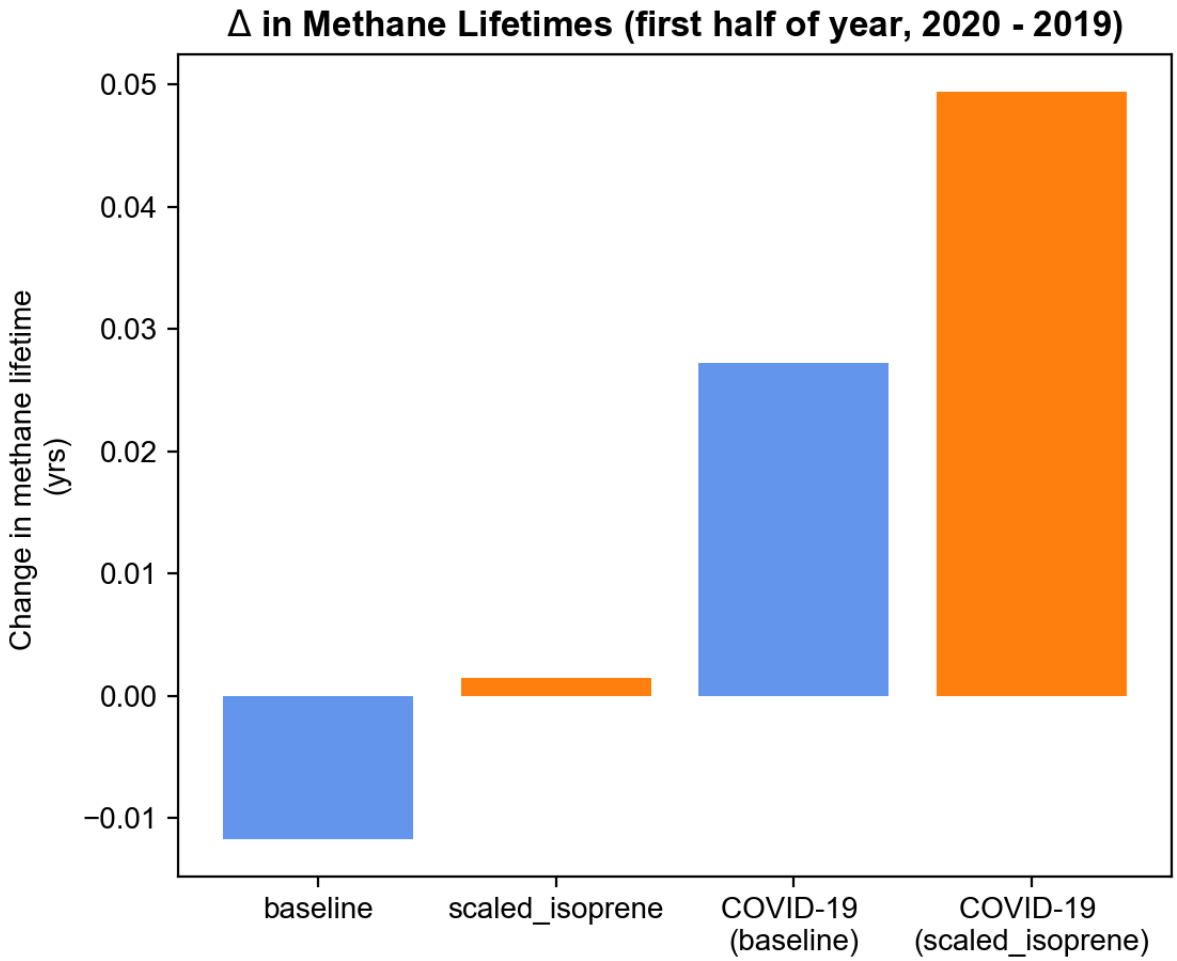

Figure 3.6: The change in methane lifetime between 2019 and 2020 for the `baseline` run (left), the `scaled_isoprene` run (middle left), the `baseline` run with COVID-19 anthropogenic NO emissions (middle right), and the `scaled_isoprene` run with COVID-19 NO emissions (right). The change in methane lifetime caused by the same NO emission perturbation is amplified by 1.2x at higher isoprene emissions (orange bars) compared to MEGAN-generated isoprene emissions (blue bars).

Chapter 4

DISCUSSION

The largest isoprene anomaly in the satellite record from CrIS occurred in 2019 and 2020, coinciding with rapid growth in methane. Here we investigated the hypothesis that increased isoprene emissions could indirectly contribute to this methane acceleration by modulating [OH] and CO. We scaled GEOS-Chem's offline isoprene emissions to better match novel CrIS isoprene retrievals, thus bringing modeled and satellite isoprene closer in agreement. The increased isoprene—and increased CO from the isoprene oxidation cascade—resulted in longer methane lifetimes due to decreased [OH]. We also show that GEOS-Chem underpredicts isoprene relative to satellite observations and that the improved agreement between MOPITT CO and the scaled run's CO suggests that this isoprene scaling is plausible. Through a combination of 0D and 3D atmospheric modeling, we show that the isoprene increase observed in the CrIS dataset during 2020 could account for 13% of 2020's methane acceleration. We obtain this value while using 2019 anthropogenic NO emissions as the 2020 values, and thus this value represents the potential impact of isoprene on the 2020 methane growth assuming no contribution from NO_x changes.

Determining the causality of this isoprene anomaly is crucial in quantifying [OH]'s response. Here, we investigate the implications of an isoprene anomaly driven solely by isoprene emissions as a potential hypothesis, but NO_x and other drivers of [OH] (e.g. actinic flux) also can influence isoprene columns observed from space. If this 2020 isoprene anomaly were driven by decreasing NO_x emissions, the observed changes in isoprene columns would be a response to the independently changing oxidative capacity, rather than isoprene being the causal agent for the [OH] changes. This different causality may influence the magnitude of the resulting [OH] perturbation, but the nonlinear relationship of the isoprene–OH-NO_x system

warrants further investigation.

Although 2020 is a special year of interest due to its methane acceleration and the potential discrepancy between MEGAN isoprene emissions and observed columns, other years within the record also experienced comparable isoprene anomalies to 2020's anomalies without similarly large perturbations to anthropogenic NO_x. Furthermore, the magnitude of these interannual variations in isoprene and their resulting impacts on [OH] are not contingent on the accuracy of our isoprene emission scaling, although our scaling can change when these variations occur. For example, even in the baseline simulation with MEGAN-generated isoprene emissions, isoprene variations cause a 0.5% decrease in global [OH] between 2014 and 2015, and a 0.1% decrease in [OH] between 2015 and 2016. Given that a 1.6% decrease in [OH] may have contributed to the unprecedented methane growth in 2020, isoprene may be an important but overlooked factor in explaining recent methane trends.

This study illustrates how isoprene can impact the global atmospheric oxidative capacity and thus methane lifetimes. We suggest that variations in isoprene, and thus changes to the biosphere, may have an important effect on the atmospheric oxidative capacity, although more research is needed to fully attribute these 2020 observations to increased isoprene emissions, decreased NO_x emissions, or changes in isoprene-NO_x chemistry. Given that isoprene emissions are driven both by short-term meteorological conditions, climate oscillations like ENSO, and long-term climate change, this mechanism may represent a potential interaction between the biosphere and the climate system mediated through atmospheric chemistry.

BIBLIOGRAPHY

[1] Ines Bamberger, Nadine K. Ruehr, Michael Schmitt, Andreas Gast, Georg Wohlfahrt, and Almut Arneth. Isoprene emission and photosynthesis during heatwaves and drought in black locust. *Biogeosciences*, 14(15):3649–3667, August 2017. Publisher: Copernicus GmbH.

[2] Kelvin H. Bates and Daniel J. Jacob. A new model mechanism for atmospheric oxidation of isoprene: global effects on oxidants, nitrogen oxides, organic products, and secondary organic aerosol. *Atmospheric Chemistry and Physics*, 19(14):9613–9640, July 2019. Publisher: Copernicus GmbH.

[3] Matthew J. Cooper, Randall V. Martin, Melanie S. Hammer, Pieternel F. Levelt, Pepijn Veefkind, Lok N. Lamsal, Nickolay A. Krotkov, Jeffrey R. Brook, and Chris A. McLinden. Global fine-scale changes in ambient NO2 during COVID-19 lockdowns. *Nature*, 601(7893):380–387, January 2022. Publisher: Nature Publishing Group.

[4] Louisa K. Emmons, Rebecca H. Schwantes, John J. Orlando, Geoff Tyndall, Douglas Kinnison, Jean-François Lamarque, Daniel Marsh, Michael J. Mills, Simone Tilmes, Charles Bardeen, Rebecca R. Buchholz, Andrew Conley, Andrew Gettelman, Rolando Garcia, Isobel Simpson, Donald R. Blake, Simone Meinardi, and Gabrielle Pétron. The Chemistry Mechanism in the Community Earth System Model Version 2 (CESM2). *Journal of Advances in Modeling Earth Systems*, 12(4):e2019MS001882, 2020. _eprint: https://onlinelibrary.wiley.com/doi/pdf/10.1029/2019MS001882.

[5] Liang Feng, Paul I. Palmer, Robert J. Parker, Mark F. Lunt, and Hartmut Bösch. Methane emissions are predominantly responsible for record-breaking atmospheric methane growth rates in 2020 and 2021. *Atmospheric Chemistry and Physics*, 23(8):4863–4880, April 2023. Publisher: Copernicus GmbH.

[6] Dejian Fu, Dylan B. Millet, Kelley C. Wells, Vivienne H. Payne, Shanshan Yu, Alex Guenther, and Annmarie Eldering. Direct retrieval of isoprene from satellite-based infrared measurements. *Nat Commun*, 10(1):3811, August 2019. Publisher: Nature Publishing Group.

[7] A. Guenther, T. Karl, P. Harley, C. Wiedinmyer, P. I. Palmer, and C. Geron. Estimates of global terrestrial isoprene emissions using MEGAN (Model of Emissions of Gases and

Aerosols from Nature). *Atmospheric Chemistry and Physics*, 6(11):3181–3210, August 2006. Publisher: Copernicus GmbH.

[8] A. B. Guenther, X. Jiang, C. L. Heald, T. Sakulyanontvittaya, T. Duhl, L. K. Emmons, and X. Wang. The Model of Emissions of Gases and Aerosols from Nature version 2.1 (MEGAN2.1): an extended and updated framework for modeling biogenic emissions. *Geoscientific Model Development*, 5(6):1471–1492, November 2012. Publisher: Copernicus GmbH.

[9] Jesse H. Kroll, Nga L. Ng, Shane M. Murphy, Richard C. Flagan, and John H. Seinfeld. Secondary Organic Aerosol Formation from Isoprene Photooxidation. *Environ. Sci. Technol.*, 40(6):1869–1877, March 2006. Publisher: American Chemical Society.

[10] X. Lan, K. W. Thoning, and E. J. Dlugokencky. Trends in globally-averaged CH4, N2O, and SF6 determined from NOAA Global Monitoring Laboratory measurements.

[11] Joshua L. Laughner, Jessica L. Neu, David Schimel, Paul O. Wennberg, Kelley Barsanti, Kevin W. Bowman, Abhishek Chatterjee, Bart E. Croes, Helen L. Fitzmaurice, Daven K. Henze, Jinsol Kim, Eric A. Kort, Zhu Liu, Kazuyuki Miyazaki, Alexander J. Turner, Susan Anenberg, Jeremy Avise, Hansen Cao, David Crisp, Joost de Gouw, Annmarie Eldering, John C. Fyfe, Daniel L. Goldberg, Kevin R. Gurney, Sina Hasheminassab, Francesca Hopkins, Cesunica E. Ivey, Dylan B. A. Jones, Junjie Liu, Nicole S. Lovenduski, Randall V. Martin, Galen A. McKinley, Lesley Ott, Benjamin Poulter, Muye Ru, Stanley P. Sander, Neil Swart, Yuk L. Yung, and Zhao-Cheng Zeng. Societal shifts due to COVID-19 reveal large-scale complexities and feedbacks between atmospheric chemistry and climate change. *Proceedings of the National Academy of Sciences*, 118(46):e2109481118, November 2021. Publisher: Proceedings of the National Academy of Sciences.

[12] Dylan B. Millet, Daniel J. Jacob, K. Folkert Boersma, Tzung-May Fu, Thomas P. Kurosu, Kelly Chance, Colette L. Heald, and Alex Guenther. Spatial distribution of isoprene emissions from North America derived from formaldehyde column measurements by the OMI satellite sensor. *Journal of Geophysical Research: Atmospheres*, 113(D2), 2008. _eprint: https://onlinelibrary.wiley.com/doi/pdf/10.1029/2007JD008950.

[13] Dylan B. Millet, Daniel J. Jacob, Solène Turquety, Rynda C. Hudman, Shiliang Wu, Alan Fried, James Walega, Brian G. Heikes, Donald R. Blake, Hanwant B. Singh, Bruce E. Anderson, and Antony D. Clarke. Formaldehyde distribution over North America: Implications for satellite retrievals of formaldehyde columns and isoprene emission. *Journal of Geophysical Research: Atmospheres*, 111(D24), 2006. _eprint: https://onlinelibrary.wiley.com/doi/pdf/10.1029/2005JD006853.

[14] Lee T. Murray, Arlene M. Fiore, Drew T. Shindell, Vaishali Naik, and Larry W. Horowitz. Large uncertainties in global hydroxyl projections tied to fate of reactive nitrogen and carbon. *Proceedings of the National Academy of Sciences*, 118(43):e2115204118, October 2021. Publisher: Proceedings of the National Academy of Sciences.

[15] NASA/LARC/SD/ASDC. MOPITT CO gridded monthly means (Near and Thermal Infrared Radiances) V009.

[16] Newton H. Nguyen, Alexander J. Turner, Yi Yin, Michael J. Prather, and Christian Frankenberg. Effects of Chemical Feedbacks on Decadal Methane Emissions Estimates. *Geophysical Research Letters*, 47(3):e2019GL085706, 2020. _eprint: https://onlinelibrary.wiley.com/doi/pdf/10.1029/2019GL085706.

[17] Nickolay A. Krotkov, Lok N. Lamsal, Sergey V. Marchenko, Edward A. Celarier, Eric J. Bucsela, William H. Swartz, Joanna Joiner, and OMI core team. OMI/Aura NO2 Cloud-Screened Total and Tropospheric Column L3 Global Gridded 0.25 degree x 0.25 degree V3, 2019.

[18] Paul I. Palmer, Dorian S. Abbot, Tzung-May Fu, Daniel J. Jacob, Kelly Chance, Thomas P. Kurosu, Alex Guenther, Christine Wiedinmyer, Jenny C. Stanton, Michael J. Pilling, Shelley N. Pressley, Brian Lamb, and Anne Louise Sumner. Quantifying the seasonal and interannual variability of North American isoprene emissions using satellite observations of the formaldehyde column. *Journal of Geophysical Research: Atmospheres*, 111(D12), 2006. _eprint: https://onlinelibrary.wiley.com/doi/pdf/10.1029/2005JD006689.

[19] Paul I. Palmer, Daniel J. Jacob, Arlene M. Fiore, Randall V. Martin, Kelly Chance, and Thomas P. Kurosu. Mapping isoprene emissions over North America using formaldehyde column observations from space. *Journal of Geophysical Research: Atmospheres*, 108(D6), 2003. _eprint: https://onlinelibrary.wiley.com/doi/pdf/10.1029/2002JD002153.

[20] Shushi Peng, Xin Lin, Rona L. Thompson, Yi Xi, Gang Liu, Didier Hauglustaine, Xin Lan, Benjamin Poulter, Michel Ramonet, Marielle Saunois, Yi Yin, Zhen Zhang, Bo Zheng, and Philippe Ciais. Wetland emission and atmospheric sink changes explain methane growth in 2020. *Nature*, 612(7940):477–482, December 2022. Publisher: Nature Publishing Group.

[21] Matthew Rigby, Stephen A. Montzka, Ronald G. Prinn, James W. C. White, Dickon Young, Simon O'Doherty, Mark F. Lunt, Anita L. Ganesan, Alistair J. Manning, Peter G. Simmonds, Peter K. Salameh, Christina M. Harth, Jens Mühle, Ray F. Weiss, Paul J. Fraser, L. Paul Steele, Paul B. Krummel, Archie McCulloch, and Sunyoung

Park. Role of atmospheric oxidation in recent methane growth. *Proceedings of the National Academy of Sciences*, 114(21):5373–5377, May 2017. Publisher: Proceedings of the National Academy of Sciences.

[22] Marielle Saunois, Ann R. Stavert, Ben Poulter, Philippe Bousquet, Josep G. Canadell, Robert B. Jackson, Peter A. Raymond, Edward J. Dlugokencky, Sander Houweling, Prabir K. Patra, Philippe Ciais, Vivek K. Arora, David Bastviken, Peter Bergamaschi, Donald R. Blake, Gordon Brailsford, Lori Bruhwiler, Kimberly M. Carlson, Mark Carrol, Simona Castaldi, Naveen Chandra, Cyril Crevoisier, Patrick M. Crill, Kristofer Covey, Charles L. Curry, Giuseppe Etiope, Christian Frankenberg, Nicola Gedney, Michaela I. Hegglin, Lena Höglund-Isaksson, Gustaf Hugelius, Misa Ishizawa, Akihiko Ito, Greet Janssens-Maenhout, Katherine M. Jensen, Fortunat Joos, Thomas Kleinen, Paul B. Krummel, Ray L. Langenfelds, Goulven G. Laruelle, Licheng Liu, Toshinobu Machida, Shamil Maksyutov, Kyle C. McDonald, Joe McNorton, Paul A. Miller, Joe R. Melton, Isamu Morino, Jurek Müller, Fabiola Murguia-Flores, Vaishali Naik, Yosuke Niwa, Sergio Noce, Simon O'Doherty, Robert J. Parker, Changhui Peng, Shushi Peng, Glen P. Peters, Catherine Prigent, Ronald Prinn, Michel Ramonet, Pierre Regnier, William J. Riley, Judith A. Rosentreter, Arjo Segers, Isobel J. Simpson, Hao Shi, Steven J. Smith, L. Paul Steele, Brett F. Thornton, Hanqin Tian, Yasunori Tohjima, Francesco N. Tubiello, Aki Tsuruta, Nicolas Viovy, Apostolos Voulgarakis, Thomas S. Weber, Michiel van Weele, Guido R. van der Werf, Ray F. Weiss, Doug Worthy, Debra Wunch, Yi Yin, Yukio Yoshida, Wenxin Zhang, Zhen Zhang, Yuanhong Zhao, Bo Zheng, Qing Zhu, Qiuan Zhu, and Qianlai Zhuang. The Global Methane Budget 2000–2017. *Earth System Science Data*, 12(3):1561–1623, July 2020. Publisher: Copernicus GmbH.

[23] Joshua D. Shutter, Dylan B. Millet, Kelley C. Wells, Vivienne H. Payne, Caroline R. Nowlan, and Gonzalo González Abad. Interannual changes in atmospheric oxidation over forests determined from space. *Science Advances*, 10(20):eadn1115, May 2024. Publisher: American Association for the Advancement of Science.

[24] Chris Smith, Zebedee R. J. Nicholls, Kyle Armour, William Collins, Piers Forster, Malte Meinshausen, Matthew D. Palmer, and Masahiro Watanabe. The Earth's Energy Budget, Climate Feedbacks, and Climate Sensitivity Supplementary Material. Technical report, 2021.

[25] A. J. Turner, D. K. Henze, R. V. Martin, and A. Hakami. The spatial extent of source influences on modeled column concentrations of short-lived species. *Geophysical Research Letters*, 39(12), 2012. _eprint: https://onlinelibrary.wiley.com/doi/pdf/10.1029/2012GL051832.

[26] Alexander J. Turner, Christian Frankenberg, Paul O. Wennberg, and Daniel J. Jacob. Ambiguity in the causes for decadal trends in atmospheric methane and hydroxyl. *Pro-*

ceedings of the National Academy of Sciences, 114(21):5367–5372, May 2017. Publisher: Proceedings of the National Academy of Sciences.

[27] Krystal T. Vasquez, John D. Crounse, Benjamin C. Schulze, Kelvin H. Bates, Alexander P. Teng, Lu Xu, Hannah M. Allen, and Paul O. Wennberg. Rapid hydrolysis of tertiary isoprene nitrate efficiently removes NOx from the atmosphere. *Proceedings of the National Academy of Sciences*, 117(52):33011–33016, December 2020. Publisher: Proceedings of the National Academy of Sciences.

[28] Violeta Velikova, Zsuzsanna Várkonyi, Milán Szabó, Liliana Maslenkova, Isabel Nogues, László Kovács, Violeta Peeva, Mira Busheva, Győző Garab, Thomas D. Sharkey, and Francesco Loreto. Increased Thermostability of Thylakoid Membranes in Isoprene-Emitting Leaves Probed with Three Biophysical Techniques. *Plant Physiology*, 157(2):905–916, October 2011.

[29] Zander S. Venter, Kristin Aunan, Sourangsu Chowdhury, and Jos Lelieveld. COVID-19 lockdowns cause global air pollution declines. *Proceedings of the National Academy of Sciences*, 117(32):18984–18990, August 2020. Publisher: Proceedings of the National Academy of Sciences.

[30] K. C. Wells, D. B. Millet, V. H. Payne, C. Vigouroux, C. a. B. Aquino, M. De Mazière, J. A. de Gouw, M. Graus, T. Kurosu, C. Warneke, and A. Wisthaler. Next-Generation Isoprene Measurements From Space: Detecting Daily Variability at High Resolution. *Journal of Geophysical Research: Atmospheres*, 127(5):e2021JD036181, 2022. _eprint: https://onlinelibrary.wiley.com/doi/pdf/10.1029/2021JD036181.

[31] Kelley C. Wells, Dylan B. Millet, Vivienne H. Payne, M. Julian Deventer, Kelvin H. Bates, Joost A. de Gouw, Martin Graus, Carsten Warneke, Armin Wisthaler, and Jose D. Fuentes. Satellite isoprene retrievals constrain emissions and atmospheric oxidation. *Nature*, 585(7824):225–233, September 2020. Publisher: Nature Publishing Group.

[32] G. M. Wolfe, J. Kaiser, T. F. Hanisco, F. N. Keutsch, J. A. de Gouw, J. B. Gilman, M. Graus, C. D. Hatch, J. Holloway, L. W. Horowitz, B. H. Lee, B. M. Lerner, F. Lopez-Hilifiker, J. Mao, M. R. Marvin, J. Peischl, I. B. Pollack, J. M. Roberts, T. B. Ryerson, J. A. Thornton, P. R. Veres, and C. Warneke. Formaldehyde production from isoprene oxidation across NO_x regimes. *Atmospheric Chemistry and Physics*, 16(4):2597–2610, March 2016. Publisher: Copernicus GmbH.

[33] Yiqi Zheng, Nadine Unger, Jovan M. Tadić, Roger Seco, Alex B. Guenther, Michael P. Barkley, Mark J. Potosnak, Lee T. Murray, Anna M. Michalak, Xuemei Qiu, Saewung

Kim, Thomas Karl, Lianhong Gu, and Stephen G. Pallardy. Drought impacts on photosynthesis, isoprene emission and atmospheric formaldehyde in a mid-latitude forest. *Atmospheric Environment*, 167:190–201, October 2017.